

Selected Paper

Shape Changes from Polygonal Gold Nanocrystals to Spherical Nanoparticles Induced by Bubbling N_2 or O_2 Gas in Polyol Synthesis of Gold Nanostructures

Md. Jahangir Alam,[1] Masaharu Tsuji,*[1,2] and Mika Matsunaga[2]

[1]Department of Applied Science for Electronics and Materials, Graduate School of Engineering Sciences, Kyushu University, Kasuga 816-8580

[2]Institute for Materials Chemistry and Engineering, Kyushu University, Kasuga 816-8580

Received August 28, 2009; E-mail: tsuji@cm.kyushu-u.ac.jp

Effects of gas bubbling in the polyol synthesis of Au nanostructures through reducing $HAuCl_4$ have been studied in an oil-bath heating at 150 °C. Under bubbling N_2, mixtures of polyhedral particles such as octahedra, triangular or hexagonal plates, and decahedra were major products (99%), besides a small amount of spherical nanoparticles (1%). Polyhedral particles were slowly transformed to monodispersed spherical particles with an average diameter of 245 ± 21 nm with increasing the heating time and the yield of spherical particles increased to 40% after heating for 60 min. When the bubbling gas was switched from N_2 to O_2, polygonal particles prepared under bubbling N_2 were rapidly etched and converted efficiently to spherical particles (96%) with an average size of 119 ± 40 nm. It was found that not only O_2 dissolved in ethylene glycol but also by-products like Cl^- anions produced in the supernatant participate in the shape changes of Au nanocrystals. The transformation of Au nanostructures under bubbling N_2 or O_2 was discussed in terms of gas bubbling induced Ostwald ripening, shape-selective oxidative etching by O_2/Cl^-, and grain-rotation-induced grain coalescence (GRIGC) and fusion mechanisms.

Recently, gold nanostructures have attracted considerable attention mainly due to their remarkable optical properties and numerous applications in fields such as catalysts, surface plasmonics, surface-enhanced Raman scattering, and chemical or biological sensing.[1–7] Since chemical and physical properties of Au nanostructures are highly related to their shapes and sizes, the shape and size control preparation of the Au nanocrystals is very important and challengeable.

The polyol reduction method is a typical chemical bottom up technique for the preparation of Au nanostructures by reducing Au^{3+} ions in the presence of a polymer surfactant such as poly(vinylpyrrolidone) (PVP) in ethylene glycol (EG).[7] Not only spherical particles, but also various polygonal nanocrystals such as octahedra, triangular or hexagonal plates, decahedra, and icosahedra with {111} facets were prepared. In general, to obtain desired shapes and sizes of Au nanostructures in high yields, Au nanoparticles were prepared by changing various experimental parameters such as concentrations of reagent (e.g., $HAuCl_4$) and surfactants (e.g., PVP), reductants and solvents (ethylene glycol or other polyols), temperatures, heating rate, heating time, heating method (oil bath or microwave heating), injection method of reagent (premix or dropwise injection), and seeded growth.[1–7] In addition to the above experimental parameters, we need to pay attention to the gaseous species from air (including O_2 and N_2) and reaction by-products. These species may influence both the reduction kinetics of a precursor and the growth rates of different crystallographic planes. However, their presence and potential roles have been largely ignored in most previous studies of the polyol synthesis of gold nanostructures.

We have recently studied effects of gas dissolved in EG for the synthesis of gold nanostructures from a mixture of $HAuCl_4 \cdot 4H_2O$/PVP/EG under oil-bath heating at 110 and 198 °C.[8] We found that both gas dissolved in reagent solution and reaction temperature gave significant effects for the shapes and sizes of final products. At 110 °C icosahedra, one-dimensional (1-D) rods and wires, and spherical particles were major products under bubbling N_2, whereas octahedra and nanoplates were dominant products under bubbling O_2. At 198 °C decahedra and icosahedra were major products under bubbling N_2, whereas the yields of larger octahedra, nanoplates, and spherical particles increased under bubbling O_2. These results showed that bubbling N_2 or O_2 gas at different temperatures can be used as a new experimental parameter for the shape- and size-controlled synthesis of Au nanostructures. It has been assumed that in a typical polyol synthesis, acetaldehyde, derived from the dehydration of EG, was the reductant. Recently Skrabalak et al.[9] reported that at least for Ag and in the temperature range of 140 to 160 °C, the primary reductant is hydroxyacetaldehyde (HA), being produced via thermal oxidation of EG by the oxygen in air.

In the present study, we have made detailed studies on effects of gas dissolved in the reagent solution for the preparation of gold nanostructures at a constant temperature of 150 °C, where HA is expected to be a dominant reductant in the presence of O_2 dissolved in EG on the basis of the previous work of Skrabalak et al. for Ag nanoparticles.[9] We found here that shapes and sizes of Au nanocrystals depend strongly on the bubbling gas and the existence of by-products produced through the decomposition of $HAuCl_4 \cdot 4H_2O$ in EG, and that

Published on the web December 18, 2009; doi:10.1246/bcsj.20090227

small polygonal nanoparticles are converted to large spherical particles under bubbling N_2 or O_2 gas. The transformation rate under bubbling N_2 was slower than that under bubbling O_2, although a narrower size distribution was obtained for the spherical particles. To the best of our knowledge this is the first study on the shape changes of Au nanostructures under bubbling gas. The growth mechanisms of different shapes and sizes of Au nanostructures under bubbling different gases were discussed in terms of gas bubbling induced Ostwald ripening, shape-selective oxidative etching by O_2/Cl^-, and grain-rotation-induced grain coalescence (GRIGC) mechanism.

Experimental

Materials. $HAuCl_4 \cdot 4H_2O$ (99.8%), NaCl (99.5%), and EG (99.5%) used for this study were purchased from Kishida Chemical Industries Ltd. The PVP powder (average molecular weight MW: 40000 in monomer units) was purchased from Wako Pure Chemical Industries Ltd. All these reagents were used without further purification. N_2 (>99.9995%), O_2 (>99.9%), and Ar (>99.9995%) gases were obtained from Taiyo Nippon Sanso Corp.

Methods. Au Nanoparticles Prepared under N_2, Ar, and O_2 Bubbling: 15 mL of EG solution was preheated to 150 °C and maintained at this temperature for 60 min by bubbling N_2, Ar, or O_2. Then a mixture of $HAuCl_4 \cdot 4H_2O$ and PVP as a polymer surfactant in 5 mL of EG was added and further heated at 150 °C for 10, 30, or 60 min by bubbling N_2, Ar, or O_2. The final concentrations of $HAuCl_4 \cdot 4H_2O$ and PVP were 2.4 and 250 mM, respectively, and the total flow rate of bubbling gas was kept at 150 sccm using mass flow controllers. Similar experiments were carried out by changing bubbling gas from N_2 to O_2 to examine effects of gases dissolved in EG.

Effects of By-products in the Supernatant Generated from the Thermal Decomposition of $HAuCl_4 \cdot 4H_2O$ under Bubbling N_2: Au nanoparticles were prepared under bubbling N_2 for 10 min using the same conditions as those described above. The products were collected by centrifugal separation at 12000 rpm three times for 30 min to remove all by-products produced in the supernatant and then a new fresh solution (250 mM PVP in 20 mL EG) was added to them. It was heated at 150 °C under bubbling O_2 for 30 or 60 min. In our experiments, small nanoparticles (<5 nm) could not be collected by centrifugal separation, when they were involved in the products. Therefore, small nanoparticles (<5 nm) were removed when the supernatant was removed.

Effects of O_2/Cl^- Oxidative Etching for Au Nanoparticles: Au nanoparticles were prepared under bubbling N_2 for 10 min using the same conditions as those shown above. The products were collected by centrifugal separation at 12000 rpm three times for 30 min and then a new fresh solution (4.8 mM NaCl and 250 mM PVP in 20 mL EG) was added. The solution was heated at 150 °C under bubbling O_2 for 30 or 60 min to examine effects of O_2/Cl^-.

Characterization. Morphologies of the Au nanoparticles were characterized using a transmission electron microscope (TEM; JEOL JEM-2010 at 200 kV). Product solutions were centrifuged at 12000 rpm three times for 30 min to ensure complete collection of the products larger than ≈5 nm each time. The precipitates were collected then re-dispersed in ethanol. Samples for TEM measurements were prepared by dropping a droplet of the colloidal solutions on the carbon-coated Cu grids. Ultraviolet–visible (UV–vis) extinction spectra were obtained (UV-3600; Shimadzu Corp.) using a quartz cell. The sample solution was diluted with EG. Aliquots of the solution were taken separately at various reaction times when the reaction was monitored by UV–vis spectra. The original solutions used for UV–vis extinction spectra detection were diluted by a factor of 8 with EG solvent. The concentrations of Cl^- and Au in supernatant of the product solutions were measured by ion chromatography (Japan DIONEX ICS-1000) and atomic absorption spectroscopy (Hitachi Z-5310), respectively.

Results and Discussion

Au Nanoparticles Prepared under Bubbling N_2, Ar, or O_2 Gas. Figures 1a1–1a3 show typical TEM images of Au nanocrystals obtained from $HAuCl_4 \cdot 4H_2O$/PVP/EG under bubbling N_2 at 150 °C for 10, 30, and 60 min, respectively. Yields and average sizes of each Au nanostructure at 10, 30, and 60 min obtained using more than three TEM images are presented in Tables 1 and 2, respectively. The yields were determined by counting the total numbers of each product and evaluating its fraction in all products. Sizes of spherical particles stand for their average diameters and the definition of sizes of other anisotropic products is shown in Figure S1 (Supporting Information). Dominant products (total 99%) at 10 min were small octahedra (42%), triangular or hexagonal plates (56%), and decahedra (1.0%). Based on TEM observations from various view angles (±15°) and their selected area electron diffraction patterns, as reported previously,[7] octahedra, triangular or hexagonal plates, decahedra, and rods have the crystal structures presented in Figure 1. In addition to a large amount of polygonal particles, a small amount of large quasi-spherical particles (1.1%) with an average diameter of 234 ± 19 nm was produced. It should be noted that with increasing the heating time from 10 min to 30 and 60 min, the total yield of small polygonal particles decreased, whereas the yield of large spherical particles increases from 1.1% to 11% and 40%, respectively. No significant changes were observed in average sizes of small polygonal nanoparticles and large spherical particles with increasing the heating time. On the basis of these findings, we concluded that small polygonal nanoparticles are converted to large spherical particles under bubbling N_2. To the best of our knowledge this is the first report that Au polygonal nanoparticles could be changed to larger spherical nanoparticles at a relatively low reaction temperature of 150 °C under polyol solvent by bubbling gas. When N_2 was replaced by Ar, similar results were obtained (Figures S2a1–S2c3′ in Supporting Information), although the conversion rate of small polygonal nanoparticles to spherical particles under bubbling Ar was slower than that under bubbling N_2.

Figures 1b1–1b3 show typical TEM images of Au nanocrystals prepared under bubbling O_2 at 150 °C for 10, 30, and 60 min, respectively. Yields and average sizes of Au nanostructures at each reaction time are given in Tables 1 and 2, respectively. It should be noted that shapes and sizes of products depend strongly on the presence of O_2. Major products (75%) were spherical particles even at 10 min and the yields of octahedra (13%), triangular and hexagonal plates (11%), and rods/wires (1.5%), were low. Most polygonal particles such as octahedra and triangular and hexagonal plates have less sharp edges/corners than those observed under bubbling N_2. With increasing the heating time from 10 min to

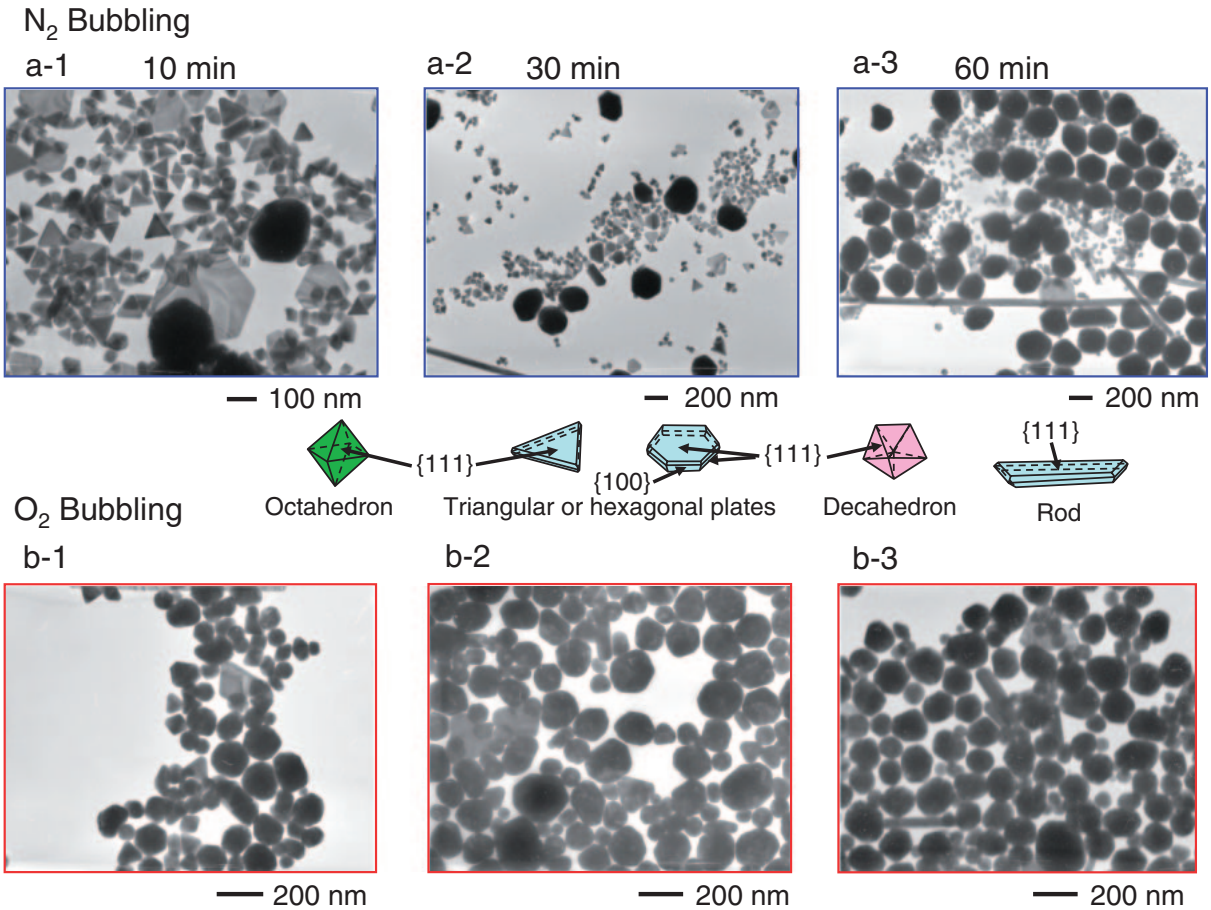

Figure 1. TEM images of Au nanostructures obtained under bubbling N_2 (a1–a3) or O_2 (b1–b3) at 150 °C in an oil-bath heating for 10, 30, and 60 min, respectively.

Table 1. Yields of Au Products (%) Obtained under Bubbling N_2 and/or O_2 at 150 °C

Bubbling gas /heating time	Octahedron	Triangular plate	Hexagonal plate	Decahedron	Rod/wire	Sphere
N_2/10 min	42	54	1.9	1.0	0.0	1.1
N_2/30 min	35	41	2.9	0.9	0.1	11
N_2/60 min	27	29	1.5	1.1	1.1	40
O_2/10 min	13	11	0.0	0.0	1.5	75
O_2/30 min	1.3	2.2	0.0	0.0	1.7	95
O_2/60 min	1.1	0.0	0.0	0.0	1.6	97
$N_2 \rightarrow O_2$/30 min	0.0	0.9	0.0	0.0	3.3	96
$N_2 \rightarrow O_2$/60 min	0.0	0.0	0.0	0.0	4.4	96
$N_2 \rightarrow O_2$ /+fresh PVP/EG 60 min	21	8.0	2.9	9.7	3.1	45
$N_2 \rightarrow O_2$ /+fresh NaCl/PVP/EG 60 min	14	34	17	8.5	5.1	21

30 and 60 min, polygonal nanoparticles were transformed to quasi-spherical particles with round edges/corners probably due to oxidative etching, so that the yield of spherical particles increased from 75% to 95% and 97%, respectively. Because of the presence of small spherical particles below 100 nm, the average size of the spheres decreases from ≈240 nm under bubbling N_2 to 100–120 nm under bubbling O_2. The average diameter of spherical particles slightly increased from 97 ± 40 nm to 105 ± 66 and 119 ± 40 nm with increasing the heating time from 10 min to 30 and 60 min, respectively.

We have previously studied the preparation of Au nanostructures under microwave (MW) heating and oil-bath heating at 198 °C (boiling point of EG) without bubbling gas.[7] It was found that polygonal particles were produced in high yields under short MW heating for 2–3 min, whereas large spherical particles were major products under oil-bath heating for 19 min.[7d] We found here for the first time that polygonal particles could also be prepared in high yields even under oil-bath heating at a lower temperature of 150 °C by bubbling inert N_2 or Ar gas.

Table 2. Average Sizes of Au Products (nm) Obtained under Bubbling N_2 and/or O_2 at 150 °C

Bubbling gas /heating time	Octahedron	Triangular plate	Hexagonal plate	Decahedron	Rod/wire	Sphere
N_2/10 min	51 ± 5	73 ± 12	175 ± 89	72 ± 12		234 ± 19
N_2/30 min	53 ± 12	71 ± 15	173 ± 59	93 ± 5	306 ± 84, 50 ± 29	240 ± 24
N_2/60 min	53 ± 13	79 ± 19	153 ± 28	79 ± 5	394 ± 29, 45 ± 15	245 ± 21
O_2/10 min	89 ± 11	106 ± 25				97 ± 40
O_2/30 min	72 ± 10	128 ± 55			154 ± 99, 62 ± 9	105 ± 66
O_2/60 min	81 ± 15				259 ± 113, 52 ± 2	119 ± 40
$N_2 \rightarrow O_2$/30 min		304 ± 35			420 ± 283, 85 ± 23	226 ± 45
$N_2 \rightarrow O_2$/60 min					743 ± 521, 98 ± 29	225 ± 36
$N_2 \rightarrow O_2$ /+fresh PVP/EG 60 min	55 ± 15	150 ± 35	625 ± 78	125 ± 22	2950 ± 1240, 82 ± 36	405 ± 87
$N_2 \rightarrow O_2$ /+fresh NaCl/PVP/EG 60 min	57 ± 18	215 ± 82	507 ± 68	108 ± 14	3530 ± 1820, 105 ± 30	331 ± 34

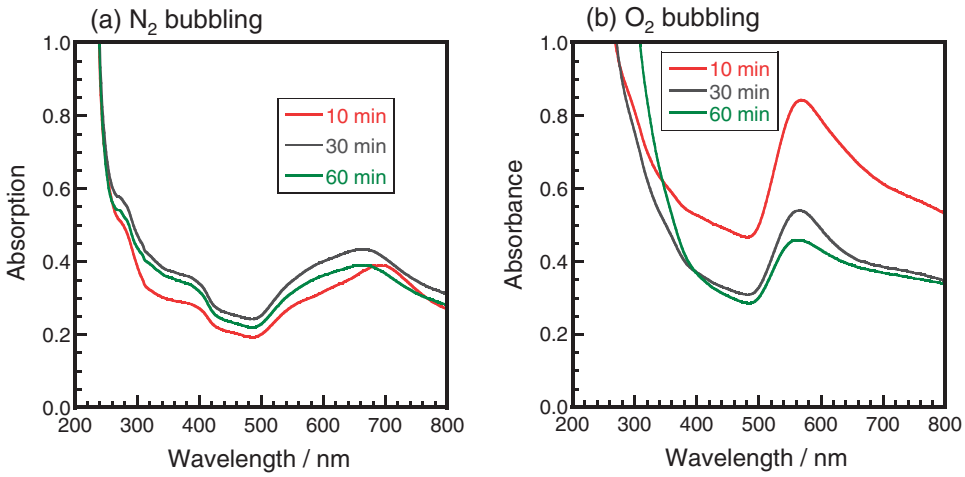

Figure 2. UV–vis spectra of product solutions obtained under bubbling N_2 (a) or O_2 (b) at different heating times.

UV–vis extinction spectra of Au solutions under bubbling N_2 or O_2 were measured to obtain information on changes in products with heating time (Figures 2a and 2b). It is known that spherical Au nanoparticles show a surface plasmon resonance (SPR) band at 520–580 nm, depending on particle sizes, whereas anisotropic Au particles show SPR bands at different peak positions depending on their shapes and sizes.[5–7] The absorption peak at 700 nm observed under bubbling N_2 for 10 min can be attributed to SPR bands of mixtures of small polygonal nanoparticles. The peak position of the SPR band shifted to blue at 660 nm with increasing the heating time from 10 to 30–60 min. The blue shift suggested that the yield of spherical particles increased with increasing the heating time. Although the peak intensity slightly increased with increasing the heating time from 10 to 30 min, it slightly decreased from 30 to 60 min.

The peak positions of SPR band under bubbling O_2 shifted to blue in comparison with those observed under bubbling N_2. It has a peak at 560 nm in the 10–60 min range mainly due to spherical Au nanoparticles. The peak intensity decreased with increasing heating time and the width of SPR band became broad. This indicates that the yield of spherical particles with wider size distributions increased with increasing heating time.

Au Nanoparticles Prepared by Changing Bubbling Gas from N_2 to O_2 or from O_2 to N_2. We found that there are large differences in shapes and sizes of Au nanostructures under bubbling N_2 or O_2, and that shapes of products change with increasing heating time. To examine more clearly whether polygonal nanoparticles are transformed to spherical particles under bubbling O_2, at first small polygonal nanoparticles were prepared under bubbling N_2, and then bubbling gas was changed from N_2 to O_2. Figures 3a–3c show typical TEM images of Au nanoparticles sampled under bubbling N_2 gas for 30 min and after changing bubbling gas from N_2 to O_2 and heating the solution for 30 or 60 min. The sample prepared under bubbling N_2 for 30 min consisted of a large number of small polygonal nanoparticles. When these products were heated under bubbling O_2 for 30 and 60 min, most polygonal particles were converted to spherical particles with an average diameter of ≈225 nm (Tables 1 and 2). Although a small amount of rods and wires was observed, little shape changes were observed for these one-dimensional (1-D) products after heating for 30–60 min. On the basis of these findings, we had definite evidence that small polygonal nanoparticles are completely transformed to spherical particles with average sizes of ≈225 nm under bubbling O_2. A comparison between Figures 1 and 3 demonstrates that shapes changes from polygonal particles to spherical ones are greatly accelerated

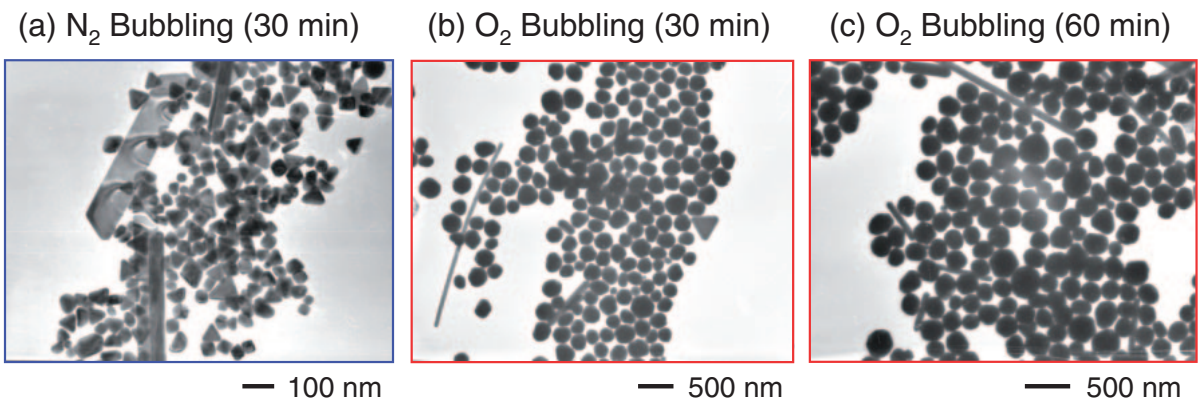

Figure 3. TEM images of Au nanostructures obtained at 150 °C in an oil-bath heating under bubbling N_2 for 30 min (a) and changing bubbling gas to O_2 for 30 (b) and 60 min (c).

in the presence of O_2 gas dissolved in EG, because all polygonal nanoparticles were rapidly transformed to spherical particles within 30 min under bubbling O_2. It should be noted that the average size of spherical nanoparticles under bubbling O_2 (100–120 nm) is smaller than that obtained under bubbling N_2 (235–245 nm) and that its standard deviation in the former experiment (40–66 nm) is larger than that in the latter (19–24 nm).

We have also made a gas change experiment from O_2 to N_2 under similar conditions. Little changes in shapes and sizes of spherical particles prepared under bubbling O_2 were observed after changing bubbling gas from O_2 to N_2 and heating for 30 and 60 min. This result implies that spherical particles with average sizes of 100–250 nm are stable at 150 °C under bubbling both N_2 and O_2 gases.

Effects of Such a By-product as Cl^- Prepared through $HAuCl_4 \cdot 4H_2O$ in Shape Conversion from Polygonal Particles to Spherical Particles. We found that polygonal particles are converted to spherical particles very rapidly under bubbling O_2. When $HAuCl_4 \cdot 4H_2O$ was reduced in EG, by-products such as Cl^- are released in the product solution. The concentration of Cl^- after heating for 10 min under bubbling N_2 or O_2 was measured to be about 3.7 mM using ion chromatography. It is generally accepted for the cases of Ag, Pd, and Pt, oxidative etching by O_2/Cl^- occurs shape selectively.[10–13] To examine effects of by-products like Cl^-, polygonal Au particles were prepared under bubbling N_2 gas, and nanoparticles were obtained by centrifugal separation of product solution. The supernatant was removed and Au products were re-dispersed in a fresh PVP(250 mM)/EG solution. Then the Au solution was heated again at 150 °C under bubbling O_2.

Figures 4a1–4a3 show typical TEM images of Au nanoparticles prepared under bubbling N_2 for 10 min and under further bubbling O_2 for 30 and 60 min in a fresh PVP/EG solution. Although the yields of large spherical and plate-like particles increased after bubbling O_2 for 30 and 60 min (Table 1), many small polygonal particles and 1-D products remain in the products (see also Figure S3 in Supporting Information, where the presence of small polygonal particles are clearly shown in magnified TEM images.). The average sizes after heating for 60 min were 405 ± 87 nm for spherical particles and 150 ± 35 and 625 ± 78 nm for triangular and hexagonal plate-like particles, respectively (Table 2). These results show that shape transformation from polygonal to spherical particles occurs without small nanoparticles (<5 nm) and by-products in the supernatant, although their shape conversion process is different from that obtained without exchanging the supernatant, as discussed later.

Effects of Cl^- in the Shape Conversion from Polygonal Particles to Spherical Ones. To examine effects of Cl^- in the shape conversion of Au nanoparticles in more detail, a similar experiment was carried out by the addition of a small amount of NaCl to a fresh PVP(250 mM)/EG solution. Figures 4b1–4b3 show typical TEM images of Au nanoparticles prepared under bubbling N_2 for 10 min and under bubbling O_2 gas for 30 and 60 min in a fresh NaCl(4.8 mM)/PVP(250 mM)/EG solution. It should be noted that as in the case of the above experiment, the yield of large spherical particles and large hexagonal plate-like particles increased after heating for 30 and 60 min under bubbling O_2 (Table 1). Under these conditions, monodispersed spherical nanoparticles with an average diameter of 331 ± 34 nm and triangular and hexagonal plate-like particles with average sizes of 215 ± 82 and 507 ± 68 nm, respectively, were prepared (Table 2). It should be noted that a lot of small polygonal particles with sharp edges/corners remained after heating for 60 min. On the basis of the above findings, species other than Cl^- involved in the supernatant and O_2 dissolved in EG play a significant role for the shape transformation. The average diameter of spherical particles after 60 min was 331 ± 34 nm, which was smaller than that obtained in a fresh PVP(250 mM)/EG solution under bubbling O_2 (405 ± 87 nm). This implies that the presence of a small amount of Cl^- plays a significant role for the formation of monodispersed spherical nanoparticles.

Analysis of Supernatant Using Atomic Absorption Spectroscopy (AAS). We have previously studied shape selective oxidative etching of Au in EG without bubbling gas.[7f,7g] We found that although Au particles were not dissolved by the addition of HCl, they were easily dissolved in the presence of $Cl^- + AuCl_4^-$ ions:

$$2Au^0 + 2Cl^- + AuCl_4^- \rightarrow 3AuCl_2^- \quad (1)$$

To examine whether $AuCl_4^-$ is present or not under bubbling N_2 and O_2 in the supernatant, it was analyzed by AAS. When we measured Au peak using supernatant without addition of

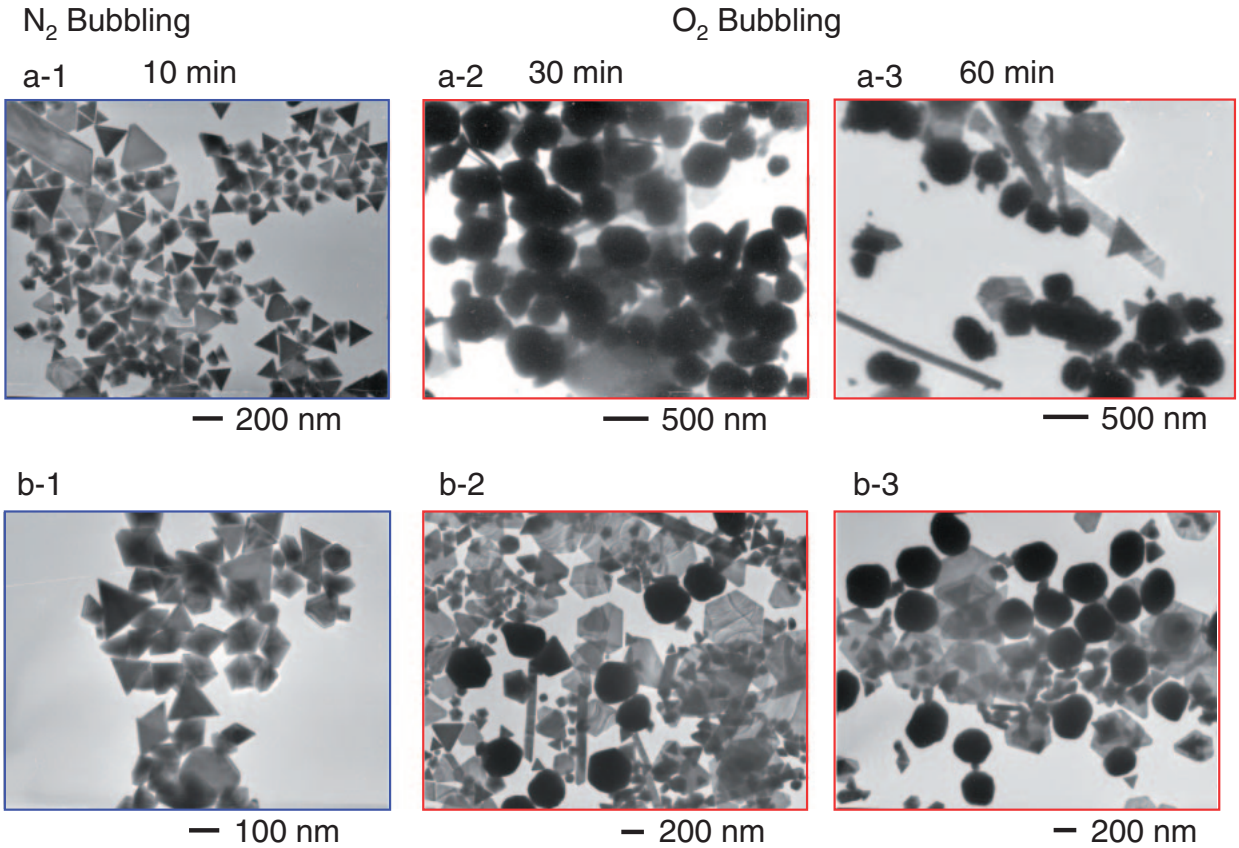

Figure 4. TEM images of Au nanostructures obtained in an oil-bath heating at 150 °C under bubbling N_2 for 10 min (a-1) and (b-1), and those obtained using fresh PVP(250 mM)/EG solution in an oil-bath heating at 150 °C under bubbling O_2 for 30 (a-2) and 60 min (a-3) and using fresh NaCl(4.8 mM)/PVP(250 mM)/EG solution at 150 °C in an oil-bath heating under bubbling O_2 for 30 (b-2) and 60 min (b-3).

any reagent like HCl, no Au peak could be observed. We confirmed that $AuCl_4^-$ could easily be detected by AAS without addition of HCl, which is involved in the standard solution of Au ions. This indicated that the concentrations of $AuCl_4^-$ and other anions involving Au were negligibly low (<0.1 ppm) in our product solutions. When we added a small amount of HCl to the supernatant, Au was detected (26 μM under bubbling N_2 gas and 0.71 μM under bubbling O_2 gas). It is known that small Au nanoparticles are dissolved by the addition of HCl leading to $AuCl_4^-$ anions because of surfaces of small nanoparticles are very active.[14] Thus, we think that these Au peaks arise from small Au nanoparticles (<5 nm), which are too small to separate using centrifugal separation at 12000 rpm. The observation of much lower concentration of Au nanoparticles under bubbling O_2 than those under bubbling N_2 is probably due to that fact that small Au nanoparticles are more easily dissolved in the solution due to oxidative etching by such etchants as Cl^- and $Cl^- + AuCl_4^-$ under bubbling O_2.

Mechanisms of Shape Transformation from Small Polygonal Nanoparticles to Spherical Particles. The growth mechanisms of Au nanostructures under different preparation routes are summarized in Figures 5 and 6. In processes 1a and 1b, a large amount of polygonal nanoparticles and a small amount of spherical particles are prepared under bubbling N_2 for 10 min and then further heated under bubbling N_2 or O_2 for 30–60 min, respectively. In process 1a, polygonal nanoparticles were slowly transformed to monodispersed spherical particles with an average diameter of ≈240 nm and polygonal particles having the same sizes as those obtained under bubbling N_2 for 10 min remained. On the other hand, when the bubbling gas was switched from N_2 to O_2, polygonal nanoparticles were rapidly transformed to monodispersed spherical particles with an average diameter of ≈225 nm and no small polygonal nanoparticles remained in the products. When Au nanostructures were prepared under bubbling O_2 for 10–60 min, spherical particles with smaller average diameters and wider distribution of 110 ± 50 nm were obtained. Large differences exist in shapes and sizes of products between process 1a and processes 1b and 2. Although small polygonal particles remained as final products in process 1a they were absent in processes 1b and 2. It is known that if nanocrystals having well-defined shapes are etched, sharp corners/edges are originally etched and gave round shapes. Due to oxidative etching, sizes of particles decrease and particles are finally dissolved in the solvent. We can observe such shapes and size changes in processes 1b and 2 with an increase in the heating time. On the other hand, no appreciable changes in shapes and sizes were observed for polygonal particles in process 1a. Thus, it is likely that process 1a and processes 1b and 2 proceed through different mechanisms.

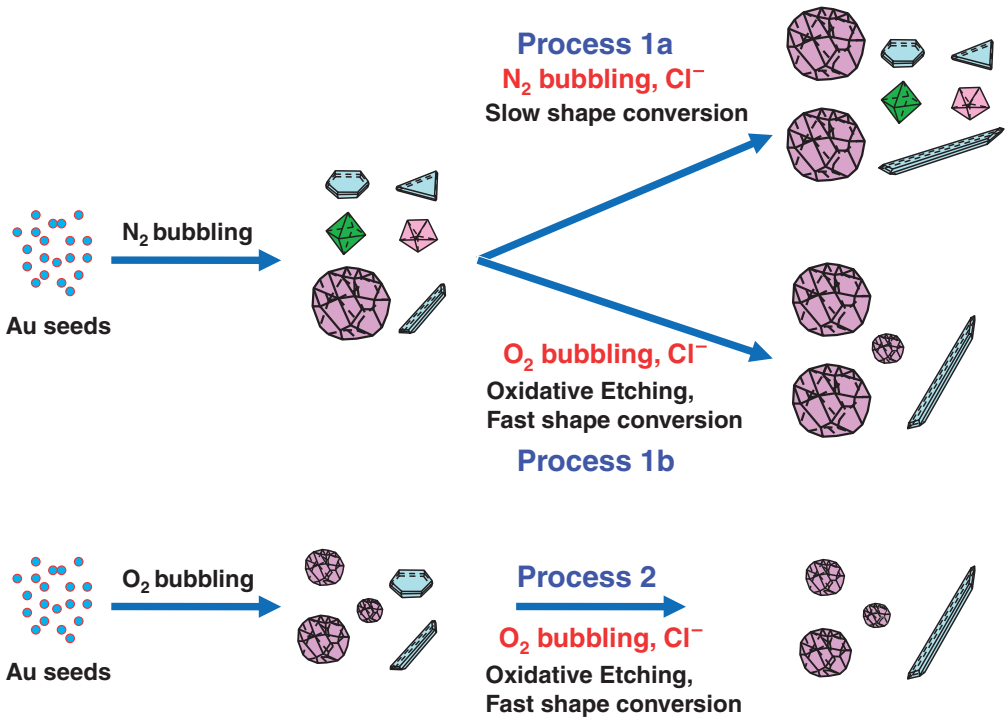

Figure 5. Growth mechanisms of Au nanostructures in an oil-bath heating at 150 °C under bubbling N_2, O_2, and by changing bubbling gas from N_2 to O_2. Cl^- anions arise from decomposition of $HAuCl_4$.

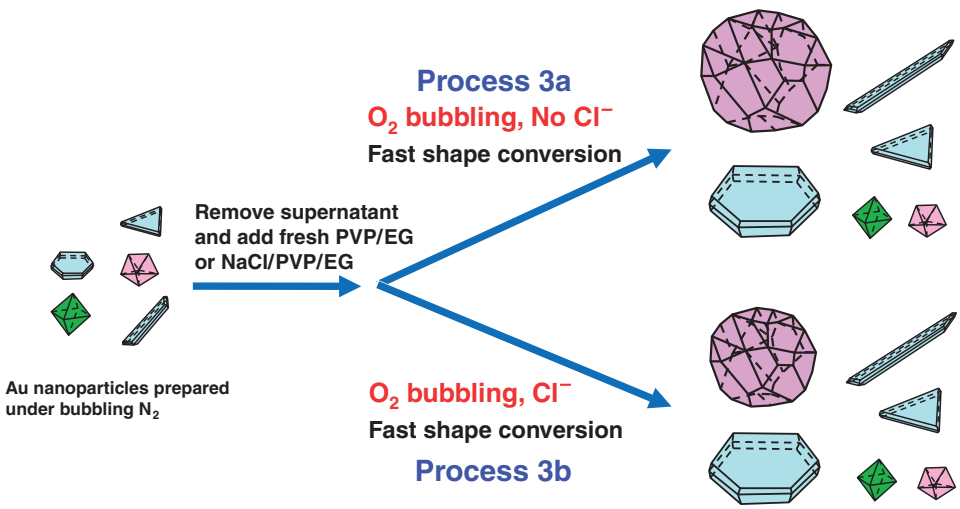

Figure 6. Growth mechanisms of Au nanostructures in an oil-bath heating at 150 °C under bubbling O_2 using fresh (a) PVP(250 mM)/EG solution and (b) NaCl(4.8 mM)/PVP(250 mM)/EG solution.

In processes 3a and 3b, we show results for effects of by-products formed in the supernatant. Processes 3a and 3b were similar to process 1b except for the supernatant. In process 3a, all by-products including Cl^- and small Au nanoparticles which were difficult to separate using centrifugal separation at 12000 rpm were removed. On the other hand, Cl^- anions were present after replacing supernatant by a fresh NaCl/PVP/EG solution in process 3b. In process 3a, polygonal nanocrystals are transformed to spherical particles with an average diameter of 405 ± 87 nm and large triangular and hexagonal plate-like particles, even though Cl^- anions were absent. In process 3b, polygonal nanoparticles were transformed to monodispersed spherical nanoparticles and large triangular and hexagonal plate-like particles. It should be noted that small polygonal nanoparticles, which are involved in the initial solution before replacing the supernatant remained in both processes 3a and 3b. This indicates that O_2 and O_2/Cl^- cannot etch Au polygonal particles, but not only O_2 but also existence of small Au nanoparticles (<5 nm) or other by-products is necessary for oxidative etching of Au polygonal particles. It seems that the shape-transformation mechanism in processes 3a and 3b is similar to that in process 1a, where the dissolution of small polygonal nanoparticles by oxidative etching is insignificant.

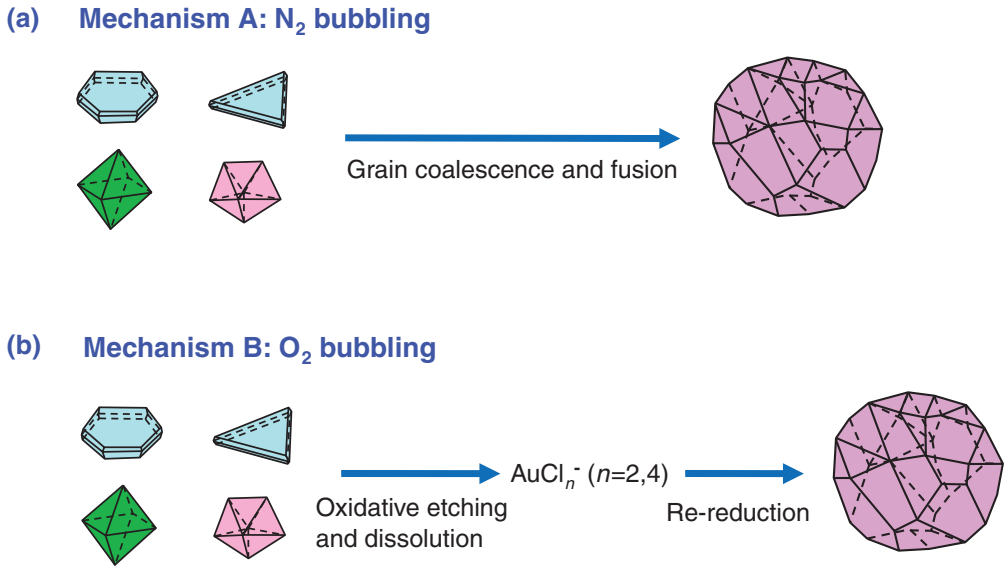

Figure 7. Proposed mechanisms of shape transformation from polygonal nanoparticles to large spherical particles using bubbling N_2 or O_2.

Based on the above findings, we propose here two typical processes for the crystal growth of large spherical particles (Figures 7a and 7b). These two processes occur to minimize total surface energies of products by reducing surface area. The major difference between the two processes is whether some parts of small particles are once dissolved to atoms or not. Mechanism A in Figure 7 is the grain-rotation-induced grain coalescence (GRIGC) and fusion mechanism,[15] where oxidative etching is not involved. Processes 1a, 3a, and 3b in Figures 5 and 6 are classified to this mechanism. According to this model, the rotation of grains among neighboring grains results in a coherent grain–grain interface which leads to the coalescence of neighboring grains via the elimination of common grain boundaries, thus forming a larger grain. In our case, single crystal, single-twin plate-like particles, and multiple-twin decahedral particles having well-defined faces were lost after the formation of large polycrystalline spherical particles. Thus, during GRIGC process fusion of polygonal crystals leading to polycrystalline spherical particles occurs.

A well-known general growth mechanism involving decreasing particles size or disappearance of smaller sizes particles is Ostwald ripening.[12e] This process may occur in processes 1b and 2. In the Ostwald-ripening mechanism, the atoms from one particle undergo dissolution and then they are transferred to another particle. There is a net atomic transport from the particles with sizes smaller than the average value to larger particles. Particles smaller than the average value will shrink or even disappear.

In the presence of O_2/Cl^- (process 3b), the yield of monodispersed spherical particles increases and that of large hexagonal plate-like particle with an average edge size of 300–500 nm increased with increasing heating time. It is generally known that it is difficult to dissolve bulk Au in HCl solution. However, Shi et al.[14] reported that small gold nanoparticles were dissolved in HCl solution and gave $AuCl_4^-$ anions. It was explained by highly active surfaces of gold. In our conditions, Au nanoparticles may also be dissolved by the Cl^- anions into $AuCl_n^-$ ($n = 2$ and 4). The lack of $AuCl_n^-$ ($n = 2$ and 4) when observed by AAS spectroscopy and UV–vis spectroscopy is explained by the fast reduction of $AuCl_n^-$ ($n = 2$ and 4) to Au^0 in EG at 150 °C leading to nucleation and growth of large spherical and plate-like particles under bubbling O_2. We found that Au nanoparticles are easily etched by $Cl^- + AuCl_4^-$ anions at low temperatures.[7f,7g] It is therefore reasonable to assume that if $AuCl_4^-$ anions are formed in the solutions, not only re-reduction of $AuCl_4^-$ to Au^0 but also etching of Au nanoparticles to $AuCl_n^-$ ($n = 2$ and 4) by Cl^- and $Cl^- + AuCl_4^-$ occurs competitively. The nucleation of Au^0 and the crystal growth provide large spherical particles. The present result implies that the oxidative etching by Cl^- and $Cl^- + AuCl_4^-$ is significantly accelerated in the presence of O_2. Under bubbling O_2, HA with a higher reduction ability than EG is formed at 150 °C. The fast reduction of $AuCl_n^-$ ($n = 2$ and 4) by HA under O_2 bubbling may be responsible for a wide size distribution of spherical nanoparticles.

In the present experiment, dissolution of Au polygonal particles was observed in processes 1b and 2 in the presence of O_2 and by-products including Cl^-. In our cases dissolution rate is sufficiently fast so that the concentration of Au atoms exceeds the supersaturation of Au atoms. In this case Au atoms themselves nucleate and provide seeds followed by crystal growth to large particles. Therefore the number of spherical particles with similar size increases. We cannot observe increase in the sizes of small numbers of spherical particles originally formed in the initial stage to very large ones due to Ostwald ripening in process 1b. Thus, we think that shape conversion of polygonal particles to large spherical particles does not arise from usual Ostwald ripening, but it comes from oxidative etching of polygonal nanoparticles and re-reduction of Au^{3+} ions to Au^0 followed by nucleation and crystal growth to large particles under bubbling O_2 in the presence of by-

products resulting from the decomposition of $HAuCl_4 \cdot 4H_2O$. This is shown as mechanism B in Figure 7. Processes 1b and 2 in Figure 5 are classified into this mechanism.

Conclusion

In summary, it is believed that shape transformation of gold nanoparticles is difficult, because gold is inactive and dissolution by oxidative etching is difficult. We found that small gold polygonal nanocrystals (50–100 nm) can be transformed to monodispersed spherical particles under bubbling N_2 or O_2. The major finding of this study is that mixtures of small polygonal nanoparticles with sharp edges could be prepared in high yields by oil-bath heating at 150 °C for 10 min under bubbling N_2 or Ar. These polygonal nanoparticles could be converted to monodispersed spherical particles under further bubbling N_2 or Ar. Although spherical Au particles can be more easily prepared under bubbling O_2 for 30–60 min, the size distribution of spherical particles were larger than that observed under bubbling N_2 or Ar.

Small nanoparticles less than 5 nm and by-products such as Cl^- formed in supernatant were found to play an important role in the shape transformation. We propose that the shape transformation proceeds through two different mechanisms depending on experimental conditions. One is the GRIGC and fusion mechanism under bubbling N_2, where monodispersed spherical particles are formed from polygonal nanoparticles by aggregation and fusion of small particles without oxidative etching. The other is oxidative etching under bubbling O_2, where polygonal particles are dissolved by oxidative etching and re-reduced to spherical particles. To confirm the validity of the above two mechanisms, further detailed experimental studies and model calculations are required.

In our experiments spherical Au particles with average diameter of ≈240 nm were formed as final products under bubbling gas in many cases, although it was unclear why they had such a sharp size distribution and crystal growth to further large particles did not occur under bubbling gases. Therefore, the gas bubbling method is a new simple technique for shape conversion of gold nanoparticles.

We thank Prof. J. Yamaki and Mrs. K. Chihara of Kyushu University for the measurements of AAS. This work was supported by the Joint Project of Chemical Synthesis Core Research Institutions, a Grant-in-Aid for Scientific Research on Priority Areas "Unequilibrium electromagnetic heating" and Grant-in-Aid for Scientific Research (B) from the Ministry of Education, Culture, Sports, Science and Technology of Japan (Nos. 19033003 and 19310064), and Kyushu Univ. GCOE program "Novel Carbon Resource Sciences." M. J. Alam thanks Kuma schorlarship for financial support.

Supporting Information

The following additional data are shown; definition of average sizes of each particle and TEM images of Au nanoparticles prepared from $HAuCl_4.4H_2O$/PVP/EG under bubbling Ar for 10–60 min and prepared from polygonal Au particles in fresh PVP(250 mM)/EG solution under bubbling O_2 for 60 min. This material is available free of charge on the web at http://www.csj.jp/journals/bcsj/.

References

1 M.-C. Daniel, D. Astruc, *Chem. Rev.* **2004**, *104*, 293.

2 B. Nikoobakht, M. A. El-Sayed, *Chem. Mater.* **2003**, *15*, 1957.

3 a) C. J. Murphy, *Science* **2002**, *298*, 2139. b) N. R. Jana, L. Gearheart, S. O. Obare, C. J. Murphy, *Langmuir* **2002**, *18*, 922. c) C. J. Murphy, T. K. Sau, A. M. Gole, C. J. Orendorff, J. Gao, L. Gou, S. E. Hunyadi, T. Li, *J. Phys. Chem. B* **2005**, *109*, 13857. d) C. J. Murphy, A. M. Gole, S. E. Hunyadi, C. J. Orendorff, *Inorg. Chem.* **2006**, *45*, 7544.

4 a) J. Rodríguez-Fernández, J. Pérez-Juste, P. Mulvaney, L. M. Liz-Marzán, *J. Phys. Chem. B* **2005**, *109*, 14257. b) A. Sánchez-Iglesias, I. Pastoriza-Santos, J. Pérez-Juste, B. Rodríguez-González, F. J. García de Abajo, L. M. Liz-Marzán, *Adv. Mater.* **2006**, *18*, 2529. c) M. Grzelczak, J. Pérez-Juste, P. Mulvaney, L. M. Liz-Marzán, *Chem. Soc. Rev.* **2008**, *37*, 1783.

5 M. Hu, J. Chen, Z.-Y. Li, L. Au, G. V. Hartland, X. Li, M. Marquez, Y. Xia, *Chem. Soc. Rev.* **2006**, *35*, 1084.

6 J. E. Millstone, S. J. Hurst, G. S. Métraux, J. I. Cutler, C. A. Mirkin, *Small* **2009**, *5*, 646.

7 a) M. Tsuji, M. Hashimoto, Y. Nishizawa, T. Tsuji, *Chem. Lett.* **2003**, *32*, 1114. b) M. Tsuji, M. Hashimoto, Y. Nishizawa, T. Tsuji, *Mater. Lett.* **2004**, *58*, 2326. c) M. Tsuji, K. Matsumoto, T. Tsuji, H. Kawazumi, *Mater. Lett.* **2005**, *59*, 3856. d) M. Tsuji, M. Hashimoto, Y. Nishizawa, M. Kubokawa, T. Tsuji, *Chem.—Eur. J.* **2005**, *11*, 440. e) M. Tsuji, N. Miyamae, S. Lim, K. Kimura, X. Zhang, S. Hikino, M. Nishio, *Cryst. Growth Des.* **2006**, *6*, 1801. f) M. Tsuji, N. Miyamae, M. Hashimoto, M. Nishio, S. Hikino, N. Ishigami, I. Tanaka, *Colloids Surf., A* **2007**, *302*, 587. g) M. Tsuji, N. Miyamae, M. Nishio, S. Hikino, N. Ishigami, *Bull. Chem. Soc. Jpn.* **2007**, *80*, 2024.

8 M. Tsuji, D. Ueyama, Md. J. Alam, S. Hikino, *Chem. Lett.* **2009**, *38*, 478.

9 S. E. Skrabalak, B. J. Wiley, M. Kim, E. V. Formo, Y. Xia, *Nano Lett.* **2008**, *8*, 2077.

10 B. Wiley, T. Herricks, Y. Sun, Y. Xia, *Nano Lett.* **2004**, *4*, 1733.

11 a) B. J. Wiley, Y. Xiong, Z.-Y. Li, Y. Yin, Y. Xia, *Nano Lett.* **2006**, *6*, 765. b) B. J. Wiley, Y. Chen, J. McLellan, Y. Xiong, Z.-Y. Li, D. Ginger, Y. Xia, *Nano Lett.* **2007**, *7*, 1032.

12 a) Y. Xiong, J. Chen, B. Wiley, Y. Xia, S. Aloni, Y. Yin, *J. Am. Chem. Soc.* **2005**, *127*, 7332. b) Y. Xiong, B. Wiley, J. Chen, Z.-Y. Li, Y. Yin, Y. Xia, *Angew. Chem., Int. Ed.* **2005**, *44*, 7913. c) N. Zettsu, J. M. McLellan, B. Wiley, Y. Yin, Z.-Y. Li, Y. Xia, *Angew. Chem., Int. Ed.* **2006**, *45*, 1288. d) Y. Xiong, H. Cai, B. J. Wiley, J. Wang, M. J. Kim, Y. Xia, *J. Am. Chem. Soc.* **2007**, *129*, 3665. e) Y. Xia, Y. Xiong, B. Lim, S. E. Skrabalak, *Angew. Chem., Int. Ed.* **2009**, *48*, 60.

13 a) M. Tsuji, Y. Nishizawa, K. Matsumoto, N. Miyamae, T. Tsuji, X. Zhang, *Colloids Surf., A* **2007**, *293*, 185. b) M. Tsuji, K. Matsumoto, N. Miyamae, T. Tsuji, X. Zhang, *Cryst. Growth Des.* **2007**, *7*, 311. c) M. Tsuji, K. Matsumoto, P. Jiang, R. Matsuo, X.-L. Tang, K. S. N. Kamarudin, *Colloids Surf., A* **2008**, *316*, 266. d) M. Tsuji, K. Matsumoto, P. Jiang, R. Matsuo, S. Hikino, X.-L. Tang, K. S. N. Kamarudin, *Bull. Chem. Soc. Jpn.* **2008**, *81*, 393. e) X. Tang, M. Tsuji, P. Jiang, M. Nishio, S.-M. Jang, S.-H. Yoon, *Colloids Surf., A* **2009**, *338*, 33. f) X. Tang, M. Tsuji, M. Nishio, P. Jiang, *Bull. Chem. Soc. Jpn.* **2009**, *82*, 1304.

14 H. Shi, H. Bi, B. Yao, L. Zhang, *Appl. Surf. Sci.* **2000**, *161*, 276.

15 E. R. Leite, T. R. Giraldi, F. M. Pontes, E. Longo, A. Beltrán, J. Andrés, *Appl. Phys. Lett.* **2003**, *83*, 1566.